Robotica: (2021) volume 39, pp. 1537–1559. © The Author(s), 2021. Published by Cambridge University Press.
doi:10.1017/S0263574720001320

Energy-Efficient Bipedal Walking: From Single-Mass Model to Three-Mass Model

Jiatao Ding†‡, Jiangchen Zhou†, Zhao Guo† and Xiaohui Xiao†*

†*School of Power and Mechanical Engineering, Wuhan University, Wuhan, Hubei Province 430072, P.R. China*
E-mails: jtding@whu.edu.cn, zhoujc@whu.edu.cn, guozhao@whu.edu.cn
‡*Shenzhen Institute of Artificial Intelligence and Robotics for Society, Shenzhen, Guangdong Province 518000, P.R. China*

(Accepted January 7, 2021. First published online: February 22, 2021)

SUMMARY
The work aims to realize energy-efficient bipedal walking by employing the three-mass inverted pendulum model (3MIPM) and compare its energy performance with linear inverted pendulum model (LIPM). To do this, a general optimal index on center of mass (CoM) acceleration is first derived for energetic cost evaluation. After defining the equivalent zero moment point (ZMP) motion, an unconstrained optimization approach for CoM generation is extended for 3MIPM, which can track different ZMP references and address the height variation as well. To make use of the allowable ZMP movement, a constrained optimization method is also employed, contributing to lower energetic cost. Simulation and hardware experiments on a humanoid robot demonstrate that the 3MIPM could achieve higher energy efficiency.

KEYWORDS: Energy efficiency; Bipedal walking; Three-mass inverted pendulum model; Allowable ZMP movement; Body height variation.

1. Introduction

Human beings walk in an energy-efficient manner, with high stability and adaptability.[1] During the past decades, advanced humanoid robots such as ASIMO,[2] Atlas,[3] and WALKMAN[4] have been developed and stable walking in real environments[5–8] has also been realized. Nevertheless, due to the limited battery capacity, the energy efficiency of locomotion still needs to be improved[9] to make humanoids practical.

For energy saving, the work on passive or under-actuated walkers[10,11] has attracted a lot of attention. However, these methods are only applicable to certain robots equipped with special structures. As a result, for example, the energy-efficient passive walkers could only walk in the flat ground or go downward slope if no other control input,[12] which could not adapt to complex real-world environments. On the contrary, various advanced methods have been reported to improve the energy efficiency of fully actuated humanoids, including those on energy storage mechanism design,[13,14] human walking or motor learning,[15–17] and gait parameters optimization,[18–22] among which the optimization-based ones are proved to be effective and easy to be generalized.

Tracking the desired distance, optimization-based approaches first evaluate the energy performance under a set of nominal step parameters and then update these parameters following the gradient that minimizes the total energetic cost. As illustrated in Fig. 1, the total energetic cost is

* Corresponding author. E-mail: xhxiao@whu.edu.cn

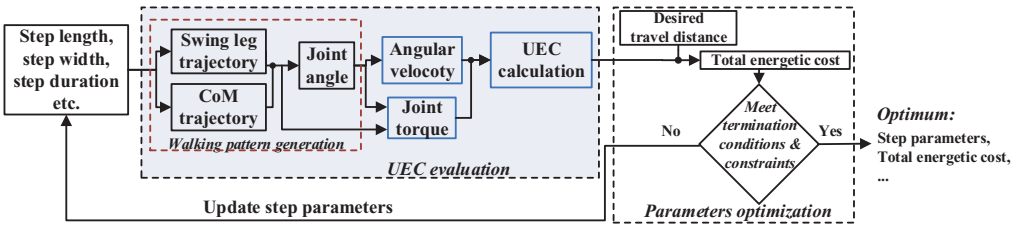

Fig. 1. Energetic cost minimization by using optimization strategies. Given a target travel distance, optimization-based approaches first evaluate the UEC under a specific set of step parameters and then update step parameters following the gradient that minimizes the total energetic cost.

determined by the unit energetic consumption (UEC) of one walking cycle. Keeping this in mind, this work concentrates on UEC performance.

As can be seen in Fig. 1, UEC evaluation is the first essential step for energy performance improvement. In terms of mechanical work evaluation, the joint power is usually chosen as the evaluation criterion (called the joint power-based index, JPI).[23–25] Since it requires obtaining joint torques and angular velocities (see Fig. 1) or electric voltage and current in advance, the calculation of JPI usually leads to a time-consuming process. Besides, it is hard to utilize the JPI to directly generate the center of mass (CoM) trajectory. When using the linear inverted pendulum model (LIPM), which assumes a lumped mass at CoM, for gait generation,[26] the UEC is actually determined by the CoM movement. Inspired by this phenomenon, the work in ref. [27] has employed the CoM work to characterize energetic cost. In refs. [28–30], the CoM trajectory was also optimized in terms of energy reduction. Nevertheless, the above work did not derive the mathematical expression between the CoM movement and the energetic cost.

Apart from UEC evaluation, different strategies can be utilized for UEC reduction. For stable walking, the zero point moment (ZMP) should be restricted within the support polygon.[31] Complying with the ZMP stability criterion, allowable ZMP region (AZR) has been employed to improve energy economy and different ZMP trajectories have been utilized, such as the linear function,[32] the sine-wave function,[33] and human-like one.[34] Furthermore, Shin et al.[35] proposed to use the fixed lateral ZMP position during single support phase (SSP) while assuming zero CoM acceleration during double support phase (DSP). Nevertheless, the above studies did not provide a theoretical explanation to answer why the ZMP movement would result in high energy efficiency. As a result, they cannot tell us which form of ZMP reference is the most efficient. In addition to the ZMP movement, body height variation (BHV) is another effective way to reduce energetic cost[36,37] and recent years have seen efforts in bipedal walking with time-varying CoM height trajectory or with a straight leg.[38–40] Although some of the above work tried to analyze the energy efficiency of BHV qualitatively, they could not either provide an explicit proof.

To overcome the above drawbacks, in previous work, that is, ref. [41], a CoM acceleration-based optimal index (CAOI) was derived. By using this cost function, an unconstrained optimization approach was proposed for CoM trajectory generation, with the capability of tracking different forms of ZMP trajectories. As a result, we provided a unified proof of the energetic benefits of AZR and BHV. Furthermore, in ref. [42], a two-stage optimization strategy was proposed to make use of the AZR. Nevertheless, all the above works are based on the LIPM, leading to large modeling errors. When the swing leg mass is large enough, the modeling error may lead to an unstable walking motion. Besides, since the LIPM does not take into consideration the upper body movement of the robot, it would result in large joint torques and low energy efficiency.[43] To address these drawbacks, researchers have extended pendulum models to take into account mass distribution, such as the two-mass IPM and the multiple-mass IPM.[44] To balance the modeling accuracy and computation complexity, Sato et al.[43,45] proposed the three-mass inverted pendulum model (3MIPM), which has attracted much attention from other researchers.[46–48] Also, efforts have been made on energy saving by using the 3MIPM, such as the work in ref. [49]. However, the work in ref. [49] utilized AZR and BHV without providing a theoretical explanation.

In this paper, we first derive the CAOI to evaluate the UEC of 3MIPM. Then, through deriving the equivalent ZMP motion of 3MIPM, the unconstrained optimization method introduced in ref. [41] is extended for generating the energy-efficient CoM trajectory, while the two-stage optimization

https://doi.org/10.1017/S0263574720001320 Published online by Cambridge University Press

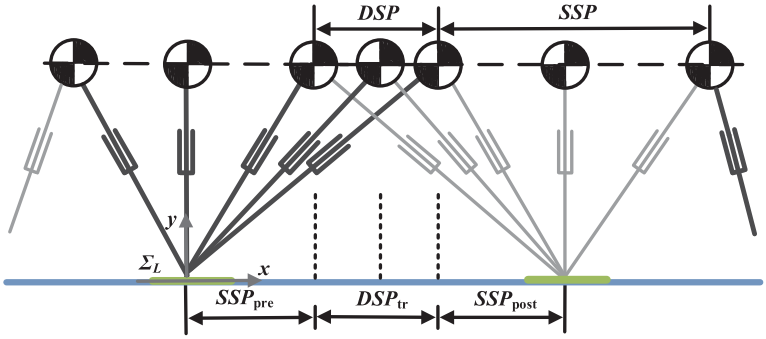

Fig. 2. Definition of the UEWC.

method[42] is employed to make use of the AZR. Finally, by modifying the step parameters inputs, higher energy economy is obtained. Compared with other work, our contribution can be concluded as follows:

(i) By analyzing the relationship of CoM movement and energetic cost, the CAOI is derived to evaluate the UEC, which is valid for LIPM and 3MIPM. Compared with the JPI function, the calculation of joint torque or joint angular velocity is not required. Furthermore, it is convenient to take the CAOI as the cost function for generating the optimal CoM trajectory.
(ii) By deriving the equivalent ZMP motion, the unconstrained optimization approach, which provides an analytic solution of the optimal CoM trajectory, is extended for 3MIPM, with the capability of tracking different forms of ZMP trajectories and addressing the BHV. Combining with the constrained ZMP trajectory optimization, minimal UEC is achieved.
(iii) The proposed CAOI provides a unified proof of the energy benefits of AZR and BHV. Besides, comparison studies reveal that, through modifying the step parameters inputs, the 3MIPM can achieve higher energy economy than LIPM.

The rest of this paper is organized as follows. In Section 2, the energetic costs of LIPM and 3MIPM are analyzed and the general CAOI for energetic cost evaluation is derived. In Section 3, by introducing the concept of equivalent ZMP, an analytic solution of the optimal upper body CoM trajectory is proposed. Besides, the constrained optimization method which adjusts the ZMP reference is introduced. Section 4 analyzes the energetic benefits of AZR and BHV. In Section 5, the energetic benefit of the proposed method is validated by hardware experiments. Section 6 draws the conclusions.

2. Energetic Consumption of Bipedal Walking

In this section, the locomotion movements of LIPM and 3MIPM are first analysed. Then, the general CAOI for UEC evaluation is proposed.

2.1. Inverted pendulum motion

Instead of using the general definition of the natural walking cycle that consists of one DSP and one consecutive SSP, we define the unit-energy walking cycle (UEWC). As illustrated in Fig. 2, the UEWC consists of one pre-half SSP (SSP_{pre}), one transitional DSP (DSP_{tr}), and one consecutive post-half SSP (SSP_{post}). During one UEWC, the origin of the local coordinate system is set to locate at the first support center.

2.1.1. LIPM motion. The LIPM motion has been analyzed in ref. [41]. Herein, we give a brief review.

The LIPM[26] assumes: (1) the robot has a lumped mass body, (2) legs are massless and telescopic, and (3) the robot moves in a constant plane. Assuming no torque input at the support foot, the orbital energy is derived as

$$\frac{1}{2}\dot{\gamma}_c^2 - \frac{\omega^2}{2}\gamma_c^2 \equiv E_{\text{orbit}}, \quad \gamma \in x, y, \tag{1}$$

https://doi.org/10.1017/S0263574720001320 Published online by Cambridge University Press

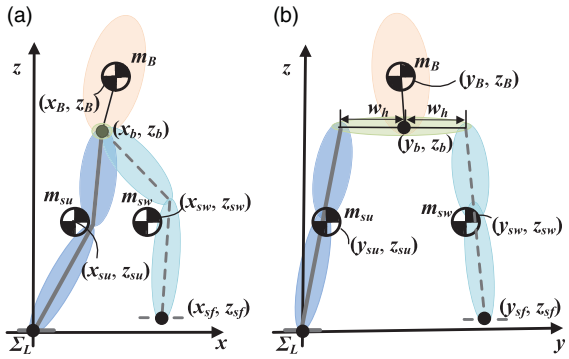

Fig. 3. 3MIPM motion, (a) sagittal plane; (b) coronal plane.

where γ_c denotes CoM displacement along x- axis (in the sagittal plane) or y- axis (in the coronal plane) and ω is the natural frequency determined by the gravitational acceleration and pendulum height.

Determined by Eq. (1), it is easy to find that the robot accelerates during SSP_{pre} whereas decelerates during SSP_{post}. Besides, it is easy to manipulate the robot to accelerate during the first half of DSP_{tr} and then to decelerate during the latter half of DSP_{tr}. As a result, considering the directions of CoM acceleration and speed, they have the same sign when t is in $[0, t_h)$ while the opposite signs when t is in $(t_h, T]$ (t_h is the middle time of one UEWC). Besides, the velocity reaches the peak at $t = t_h$. That is,

$$\begin{cases} \ddot{\gamma}_c(t)\dot{\gamma}_c(t) > 0, & 0 < t < t_h, \\ \ddot{\gamma}_c(t)\dot{\gamma}_c(t) = 0, & t = t_h, \\ \ddot{\gamma}_c(t)\dot{\gamma}_c(t) < 0, & t_h < t < T, \end{cases} \tag{2}$$

where we assume $t_h = (t_i + t_f)/2 = T/2$, t_i and t_f denote the ending time of SSP_{pre} and the starting time of SSP_{post}, respectively.

Considering the ground reaction force, the ZMP dynamics is determined by

$$\ddot{\gamma}_c = \omega^2(\gamma_c - p_\gamma), \tag{3}$$

where p_γ denotes the ZMP trajectory along x- or y-axis.

Determined by Eq. (3), Eq. (2) may not be strictly satisfied, especially when the reference ZMP moves within the support region during SSP_{pre} and SSP_{post}. However, the work in ref. [41] reveals that this stage merely lasts a short period with a low CoM velocity. Furthermore, if the ZMP movement during SSP is smaller than the step length or width, it has little impact on energy performance. Thus, we assume that Eq. (2) is satisfied during the whole UEWC.

2.1.2. 3MIPM motion. As demonstrated in Fig. 3, differing from the LIPM, the 3MIPM assumes three distributed masses, namely, upper body mass (m_B), support leg mass (m_{su}), and swing leg mass (m_{sw}). Considering the non-uniform mass distribution on different rods, we have the CoM positions during the SSP_{pre} as (taking the right support as an example)

$$\begin{cases} x_B = x_b + c_{xb}, & x_{su} = \dfrac{x_b}{2} + c_{xu}, & x_{sw} = \dfrac{x_b + x_{sf}}{2} + c_{xw}, \\ y_B = y_b + c_{yb}, & y_{su} = \dfrac{y_b - w_h}{2} + c_{yu}, & y_{sw} = \dfrac{y_b + w_h + y_{sf}}{2} + c_{yw}, \\ z_B = c_{zb}, & z_{su} = c_{zu}, & z_{sw} = c_{zw}, \end{cases} \tag{4}$$

where (x_B, y_B, z_B), (x_{su}, y_{su}, z_{su}), and (x_{sw}, y_{sw}, z_{sw}) denote the CoM position of the upper body, the support leg, and the swing leg, respectively. (x_b, y_b, z_b) and (x_{sf}, y_{sf}, z_{sf}) denote the position of the pelvis center and the position of the swing foot center, respectively. (c_{xb}, c_{yb}), (c_{xu}, c_{yu}), and

https://doi.org/10.1017/S0263574720001320 Published online by Cambridge University Press

(c_{xw}, c_{yw}) are the constant horizontal CoM offsets, which are determined by the mass distribution of links. (c_{zb}, c_{zu}, c_{zw}) are the constant CoM heights of three distributed masses.

According to the definition of the UEWC, the first support leg would not transform to be the next swing leg until DSP_{tr} ends. As a result, during the DSP_{tr}, we have following constraints

$$x_{sf} = S_x, \quad y_{sf} = S_y, \tag{5}$$

where S_x and S_y separately denote the desired step length and step width.

Besides, during the SSP_{post}, the 3MIPM motion is also determined by slightly modifying the Eq. (4), which is not discussed in detail. As a result, the CoM movements of the distributed masses can be characterized by the motions of the pelvis center and the swing foot center, which would be used for UEC modeling and gait generation.

2.2. *CAOI for UEC evaluation*

Ignoring the friction work and assuming no body rotation, the UEC is represented by the energy input for tracking the reference CoM trajectory. Besides, since the vertical CoM motion is driven by conservative gravitational force, only the energy input for horizontal CoM movement is considered. Note that, since we aim to evaluate the energetic cost rather than calculating it accurately at this stage, above simplifications are acceptable, which would be demonstrated in following sections.

2.2.1. UEC evaluation for LIPM. Based on the above simplifications, when using the LIPM, the UEC is determined by the energy input for driving the lumped mass to track the reference CoM trajectory. Given the total mass (m_c), we have

$$E_{\text{nom}} = \int_0^T |F_\gamma(t)\dot{\gamma}_c(t)|dt = m_c \int_0^T |\ddot{\gamma}_c(t)\dot{\gamma}_c(t)|dt, \tag{6}$$

where $F_\gamma(t)$ denotes the force acting on the lumped mass.

Using Eq. (2), Eq. (6) can be simplified to be following integral form:

$$\begin{aligned} E_{\text{int}} &= \int_0^{t_h} \ddot{\gamma}_c(t)\dot{\gamma}_c(t)dt - \int_{t_h}^T \ddot{\gamma}_c(t)\dot{\gamma}_c(t)dt \\ &= \frac{1}{2}\left(\left[(\dot{\gamma}_c(t_h))^2 - (\dot{\gamma}_c(0))^2\right] + \left[(\dot{\gamma}_c(t_h))^2 - (\dot{\gamma}_c(T))^2\right]\right). \end{aligned} \tag{7}$$

Noting that, for time $t < t_h$, the CoM velocity increases monotonically. After t_h, the CoM velocity decreases monotonically. We can make the following reasonable inferences

$$|\dot{\gamma}_c(t_h)| >> |\dot{\gamma}_c(0)|, \quad |\dot{\gamma}_c(t_h)| >> |\dot{\gamma}_c(T)|. \tag{8}$$

As a result, the reduction of Eq. (7) can be further simplified to be minimizing the following CAOI

$$J_{\text{c}} = \min\left[\int_0^T (\ddot{\gamma}_t)^T (\ddot{\gamma}_t)\, dt\right]. \tag{9}$$

Since the nominal energetic cost (E_{nom} in Eq. (6)) and the CAOI (J_{c} in Eq. (9)) can be calculated by merely analyzing the CoM movement, we can evaluate the energy performance of the LIPM without computing joint angles or torques in advance.

2.2.2. UEC evaluation for 3MIPM. Similar to the LIPM, by using the above simplifications, the energetic cost of the 3MIPM is determined by the energy inputs for driving the three masses to track the reference trajectories. Thus, given the distributed masses (m_B, m_{su} and m_{sw}), the nominal UEC of the 3MIPM (E^3_{nom}) is determined as

$$\begin{aligned} E^3_{\text{nom}} &= E^B_{\text{nom}} + E^{su}_{\text{nom}} + E^{sw}_{\text{nom}} \\ &= m_B \int_0^T |\ddot{\gamma}_B(t)\dot{\gamma}_B(t)|dt + m_{su} \int_0^T |\ddot{\gamma}_{su}(t)\dot{\gamma}_{su}(t)|dt + m_{sw} \int_0^T |\ddot{\gamma}_{sw}(t)\dot{\gamma}_{sw}(t)|dt, \end{aligned} \tag{10}$$

https://doi.org/10.1017/S0263574720001320 Published online by Cambridge University Press

where E^{B}_{nom}, E^{su}_{nom}, E^{sw}_{nom} represent the nominal energetic cost needed by the upper body movement, the support leg movement, and the swing leg movement, respectively; γ_{B}, γ_{su}, γ_{sw} denote the CoM trajectories of three masses along $x-$ or $y-$ axis, respectively.

As can be seen from Eq. (10), the E^{3}_{nom} is determined by the CoM velocities and accelerations of three distributed masses. Based on analyses in Section 2.1.2, the velocities and accelerations of different masses are determined by those of pelvis center and swing foot center. Thus, we have (assuming the right support during the SSP_{pre})

$$\begin{aligned}
E^{B}_{\text{nom}} &= m_{B}\int_{0}^{T}|\ddot{\gamma}_{b}(t)\dot{\gamma}_{b}(t)|dt,\\
E^{su}_{\text{nom}} &= m_{su}\int_{0}^{T}\left|\frac{\ddot{\gamma}_{b}(t)\dot{\gamma}_{b}(t)}{4}\right|dt,\\
E^{sw}_{\text{nom}} &= m_{sw}\left(\int_{0}^{t_i}\left|\frac{\left(\ddot{\gamma}_{b}(t)+\ddot{\gamma}_{sf}(t)\right)\left(\dot{\gamma}_{b}(t)+\dot{\gamma}_{sf}(t)\right)}{4}\right|dt+\int_{t_i}^{t_f}\left|\frac{\ddot{\gamma}_{b}(t)\dot{\gamma}_{b}(t)}{4}\right|dt\right.\\
&\quad\left.+\int_{t_f}^{T}\left|\frac{\left(\ddot{\gamma}_{b}(t)+\ddot{\gamma}_{sf}(t)\right)\left(\dot{\gamma}_{b}(t)+\dot{\gamma}_{sf}(t)\right)}{4}\right|dt\right),
\end{aligned}\tag{11}$$

where γ_{b}, γ_{sf} denote the horizontal trajectories of the pelvis center and the swing foot center along the $x-$ or $y-$ axis, respectively.

Thus, the problem is, *determined by Eq.* (11)*, finding solutions so that the Eq.* (10) *achieves the minimum*.

It comes first that, for kinematic calculation, the horizontal movement of the pelvis center $(x_{b},\ y_{b})$ in the 3MIPM plays the same role with the horizontal CoM movement in the LIPM. Therefore, we assume that the motion properties expressed in Eqs. (2) and (8) are also satisfied by the pelvis center motion in 3MIPM during the whole UEWC. As a result, the E^{B}_{nom} and E^{su}_{nom} expressed in Eq. (11) can achieve the minimum by minimizing the acceleration of the pelvis center during the whole UEWC.

Then, E^{sw}_{nom} can be minimized by planning the trajectory of the swing foot center. Following the definition of UEWC, in the sagittal plane, the swing foot center decelerates from the maximal velocity to zero velocity during the SSP_{pre}. During the SSP_{post}, the swing foot center accelerates from zero velocity to the maximal velocity. Thus, we have (assuming the robot moves forward):

$$\begin{cases}\dot{\gamma}_{sf}(t)\geq 0, & \ddot{\gamma}_{sf}(t)\leq 0, \quad 0<t<t_i,\\ \dot{\gamma}_{sf}(t)\geq 0, & \ddot{\gamma}_{sf}(t)\geq 0, \quad t_f<t<T.\end{cases}\tag{12}$$

On the other hand, the lateral movement of the swing foot center has zero velocity and zero acceleration when no lateral displacement is desired, which is the most common case. Thus, in the coronal plane, the energy consumed by the swing leg is merely determined by the pelvis movement. Inspired by this phenomenon, to further reduce the energetic cost caused by the swing leg sway, we also expect the zero acceleration in the sagittal trajectory of the swing foot center, which can be used to guide the trajectory generation. Actually, in order to avoid rigid impact with the ground, we can design the sagittal trajectories of the swing foot center during the SSP_{pre} and SSP_{post} by using the 2^{nd} order polynomials. As a result, the acceleration of the swing foot center achieves the minimum during the SSP_{pre} and SSP_{post}. In the case, the E^{sw}_{nom} in Eq. (11) can be further simplified as (E^{sw}_{sim})

$$\begin{aligned}
E^{sw}_{\text{sim}} &= m_{sw}\left(\int_{0}^{t_i}\left|\frac{\ddot{\gamma}_{b}(t)(\dot{\gamma}_{b}(t)+\dot{\gamma}_{sf}(t))}{4}\right|dt+\int_{t_i}^{t_f}\left|\frac{\ddot{\gamma}_{b}(t)\dot{\gamma}_{b}(t)}{4}\right|dt\right.\\
&\quad\left.+\int_{t_f}^{T}\left|\frac{\ddot{\gamma}_{b}(t)(\dot{\gamma}_{b}(t)+\dot{\gamma}_{sf}(t))}{4}\right|dt\right).
\end{aligned}\tag{13}$$

Considering the motion property expressed in Eq. (12), we have $\dot{\gamma}_{sf}(t)\geq 0$ during the whole UEWC. Also, talking the forward movement as an example, we have $\dot{\gamma}_{b}(t)\geq 0$ during the whole

https://doi.org/10.1017/S0263574720001320 Published online by Cambridge University Press

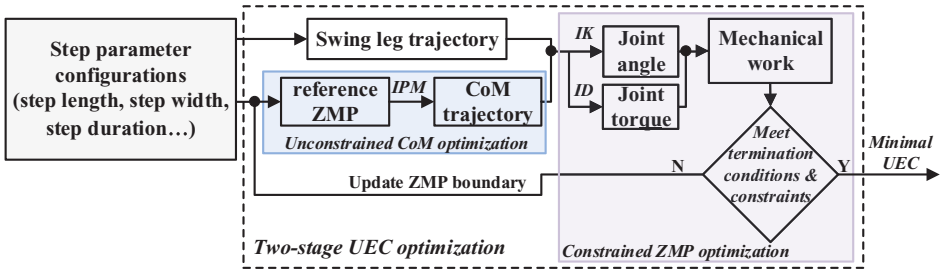

Fig. 4. Two-stage optimization for UEC reduction.

UEWC. Then, by utilizing the inference in Eq. (8), the *necessary condition* when Eq. (13) achieves the minimum is that the global pelvis acceleration achieves the minimum.

As a result, the pelvis acceleration should be reduced to minimize the total UEC in Eq. (10). Therefore, the CAOI for 3MIPM is proposed as

$$J_c^{3m} = \min\left[\int_0^T (\ddot{\gamma}_b(t))^T (\ddot{\gamma}_b(t))dt\right]. \tag{14}$$

As can be seen from Eqs. (9) and (14), a unified CAOI is proposed for energetic cost evaluation. Although there is no strict mathematical proof, the following sections demonstrate that the CAOI is valid when using LIPM or 3MIPM. Again, using this function, there is no need to calculate the joint torques and angular velocities in advance. Furthermore, CAOI can also be used for directly generating optimal CoM trajectory.

3. Two-stage Optimization for UEC Reduction

Using the proposed CAOI (9), a fast unconstrained optimization method was proposed in ref. [41] to solve the optimal CoM trajectory following the reference ZMP, which provides an analytic solution. After that, the constrained ZMP optimization was taken into consideration in ref. [42], leading to a two-stage optimization process. In this section, focusing on the 3MIPM, we first derive the equivalent ZMP motion. Then, we extend the two-stage optimization method for UEC reduction. As illustrated in Fig. 4, the unconstrained CoM optimization is adopted at the first stage to obtain the optimal upper body CoM trajectory of 3MIPM. Then, at the second stage, the AZR is exploited by a constrained optimization strategy.

3.1. 3MIPM dynamics

Using the 3MIPM, the ZMP trajectories are calculated by

$$p_\gamma^{3m} = \frac{\sum_\xi^{B,su,sw} m_\xi\left(\left(\ddot{z}_\xi + g\right)\gamma_\xi - z_\xi\ddot{\gamma}_\xi\right)}{\sum_\xi^{B,su,sw} m_\xi\left(\ddot{z}_\xi + g\right)}, \tag{15}$$

where p_γ^{3m} denote the ZMP trajectory along $x-$ or $y-$ axis.

After defining the reference ZMP trajectory and swing foot trajectory, the position of the pelvis center is determined by Eq. (15). Since we assume the constant horizontal CoM offsets and the constant CoM heights, the 3MIPM dynamics can be simplified as

$$\ddot{\gamma}_b = \left(w^{\text{eq}}\right)^2\left(\gamma_b - p_\gamma^{\text{eq}}\right), \tag{16}$$

where the equivalent ZMP (p_γ^{eq}) and equivalent natural frequency (w^{eq}) are

$$\begin{aligned} p_\gamma^{\text{eq}} &= \frac{m_c}{m_b + m_L}\left[p_\gamma^{3m} - e_\gamma - \frac{m_L}{2m_c}\left(\gamma_{sw} - \frac{c_{zw}}{g}\ddot{\gamma}_{sw}\right)\right], \\ w^{\text{eq}} &= \sqrt{\frac{g(m_B + m_L)}{e_z m_c}}, \end{aligned} \tag{17}$$

https://doi.org/10.1017/S0263574720001320 Published online by Cambridge University Press

where $m_{_L}$ denotes the leg mass and $m_{_L} = m_{su} = m_{sw}$, m_c is the total mass and $m_c = m_{_B} + 2m_{_L}$, the e_x, e_y and e_z are calculated by

$$e_\iota = \frac{m_{_B} c_{\iota b} + m_{_L} c_{\iota u} + m_{_L} c_{\iota w}}{m_c}, \iota \in x, y, z \tag{18}$$

As can be seen from Eq. (16), the CoM trajectory of the upper body in the 3MIPM is determined by the equivalent ZMP trajectory. In fact, assuming the zero leg mass, Eq.(18) coincides with Eq. (3). Note that, even the vertical height varies during one UEWC, (16) can still be satisfied when there is zero vertical CoM acceleration, meaning that the specific form of vertical height variation can be addressed, which would be discussed in details in Section 4.

3.2. Unconstrained CoM trajectory optimization

Any solver minimizing the CAOI can be used to generate the energy-efficient CoM trajectory. In ref. [41], using the LIPM, we modified the work in ref. [30] and proposed an unconstrained optimization method, which could deal with different forms of ZMP references. Herein, by introducing the equivalent ZMP, the approach can also work well for generating the optimal pelvis center trajectory of 3MIPM. Taking the LIPM motion as an example, this section gives a brief overview of this method.

3.2.1. Problem statement. Changing the coordinates, we have following dynamical model,

$$\begin{bmatrix} \dot{\gamma}_{\mathrm{u}} \\ \dot{\gamma}_{\mathrm{s}} \end{bmatrix} = \begin{bmatrix} \omega & 0 \\ 0 & -\omega \end{bmatrix} \begin{bmatrix} \gamma_{\mathrm{u}} \\ \gamma_{\mathrm{s}} \end{bmatrix} + \begin{bmatrix} -\omega \\ \omega \end{bmatrix} p_\gamma. \tag{19}$$

where γ_{u} and γ_{s} are the unstable component and stable component of the CoM motion along the $x-$ or $y-$axis, as defined in ref. [50].

Thus, the problem is, *given the reference ZMP during* SSP_{pre} *and* SSP_{post}, *obtaining the optimal CoM trajectory by minimizing the CAOI*. According to refs. [29] and [30], to track a reference ZMP, following solutions exist:

$$\begin{cases} \gamma_{\mathrm{u}}^* = \omega \int_0^\infty e^{-\omega\tau} p_\gamma(t+\tau) d\tau, \\ \gamma_{\mathrm{s}}^* = \omega \int_0^\infty e^{-\omega\tau} p_\gamma(t-\tau) d\tau. \end{cases} \tag{20}$$

Herein, note $e_{\mathrm{u}} = \gamma_{\mathrm{u}} - \gamma_{\mathrm{u}}^*$ and $e_{\mathrm{s}} = \gamma_{\mathrm{s}} - \gamma_{\mathrm{s}}^*$, the CoM trajectory can be solved by

$$\gamma_c = \frac{1}{2}(\gamma_{\mathrm{u}} + \gamma_{\mathrm{s}}) = \gamma_c^* + \frac{1}{2}(e_{\mathrm{u}} + e_{\mathrm{s}}). \tag{21}$$

After defining the reference ZMP, the γ_c^* can be calculated by using Eq. (20) and the optimal CoM is determined by e_{u} and e_{s}.

3.2.2. Analytic solution derivation. Following the definition of UEWC, the CoM trajectory is divided into three segments, namely, the CoM trajectories during SSP_{pre}, DSP_{tr}, and SSP_{pre}. For the brevity, we only discuss the CoM motion during the SSP_{pre} in detail.

During SSP_{pre}, we have the final condition at $t = t_i$. The error dynamics is solved as

$$\begin{bmatrix} e_{\mathrm{u}}(t) \\ e_{\mathrm{s}}(t) \end{bmatrix} = \begin{bmatrix} e^{-\omega(t_i - t)} & 0 \\ 0 & e^{\omega(t_i - t)} \end{bmatrix} \begin{bmatrix} e_{\mathrm{u}}(t_i) \\ e_{\mathrm{s}}(t_i) \end{bmatrix}. \tag{22}$$

Considering following final condition $e_{\mathrm{s}}(t_i) \equiv 0$, the CoM trajectory in Eq. (21) can be given as

$$\gamma_c(t) = \frac{1}{2} e^{-\omega(t_i - t)} \left[\gamma_{\mathrm{u}}(t_i) - \gamma_{\mathrm{u}}^*(t_i)\right] + \gamma_c^*(t). \tag{23}$$

https://doi.org/10.1017/S0263574720001320 Published online by Cambridge University Press

Then, the CoM acceleration can be rewritten as

$$\begin{aligned}\ddot{\gamma}_c^{\text{pre}}(t) &= \frac{\omega^2}{2}[e_{\text{u}}(t) + e_{\text{s}}(t)] + \omega^2\left[\gamma_c^*(t) - p_\gamma(t)\right] \\ &= \frac{\omega^2}{2}e_{\text{u}}(t) + \omega^2[\gamma_c^*(t) - p_\gamma(t)].\end{aligned} \tag{24}$$

Defining $p_\gamma(t) = \sum_{i=0}^{2} \alpha_i t^i$ during SSP_{pre} and SSP_{post}, we have

$$\gamma_c^*(t) - p_\gamma(t) = \frac{2\alpha_2^i}{\omega^2}, \tag{25}$$

where α_2^i denotes the quadratic coefficient for the SSP_{pre}.

Finally, we can calculate the optimal quadratic index as

$$\begin{aligned}J_{\text{pre}} &= \int_0^{t_i} (\ddot{\gamma}_c(t))^T(\ddot{\gamma}_c(t))dt \\ &= \int_0^{t_i} \left[\frac{\omega^2}{2}e^{-\omega(t_i - t)}e_{\text{u}}(t_i) + 2\alpha_2^i\right]^2 dt \\ &= \frac{\omega^3}{8}\left(1 - e^{-2\omega t_i}\right)[e_{\text{u}}(t_i)]^2 + 2\alpha_2^i\omega\left(1 - e^{-\omega t_i}\right)e_{\text{u}}(t_i) + \Delta_{\text{pre}} \\ &= W_1[e_{\text{u}}(t_i)]^2 - 2H_1 e_{\text{u}}(t_i) + \Delta_{\text{pre}},\end{aligned} \tag{26}$$

where W_1 and H_1 separately denote the coefficients of the second-order term and the first-order term, Δ_{pre} is the constant term.

Denoting $\Psi = [\gamma_{\text{u}}(t_i), \gamma_{\text{s}}(t_f)]^T$, $\mathbf{F}_{\text{pre}} = [\gamma_{\text{u}}^*(t_i), \gamma_{\text{s}}^*(t_i)]^T$,

$$\begin{aligned}J_{\text{pre}} &= \Psi^T\begin{bmatrix} W_1 & 0 \\ 0 & 0 \end{bmatrix}\Psi - 2\Psi^T\left(\begin{bmatrix} W_1 & 0 \\ 0 & 0 \end{bmatrix}\mathbf{F}_{\text{pre}} + \begin{bmatrix} H_1 \\ 0 \end{bmatrix}\right) + \Delta_{\text{pre}} \\ &= \Psi^T\mathbf{W}_{\text{pre}}\Psi - 2\Psi^T\mathbf{H}_{\text{pre}} + \Delta_{\text{pre}}.\end{aligned} \tag{27}$$

Similarly, during the SSP_{post} and DSP_{tr}, we have

$$\begin{aligned}J_{\text{post}} &= \Psi^T\mathbf{W}_{\text{post}}\Psi - 2\Psi^T\mathbf{H}_{\text{post}} + \Delta_{\text{post}}, \\ J_{\text{tr}} &= \Psi^T\mathbf{W}_{\text{tr}}\Psi - 2\Psi^T\mathbf{H}_{\text{tr}} + \Delta_{\text{tr}},\end{aligned} \tag{28}$$

where $[\mathbf{W}_{\text{post}}, \mathbf{W}_{\text{tr}}]^T$, $[\mathbf{H}_{\text{post}}, \mathbf{H}_{\text{tr}}]^T$, and $[\Delta_{\text{post}}, \Delta_{\text{tr}}]^T$ separately denote the Hessian matrices, coefficient matrices of the first term and the constant terms during the SSP_{post} and DSP_{tr}. More details can be found in ref. [41].

Finally, global optimal index is derived as

$$J_{\text{c}} = J_{\text{pre}} + J_{\text{tr}} + J_{\text{post}} = \Psi^T\mathbf{W}\Psi - 2\Psi^T\mathbf{H} + \Delta, \tag{29}$$

where $\mathbf{W} = \mathbf{W}_{\text{pre}} + \mathbf{W}_{\text{tr}} + \mathbf{W}_{\text{post}}$, $\mathbf{H} = \mathbf{H}_{\text{pre}} + \mathbf{H}_{\text{tr}} + \mathbf{H}_{\text{post}}$, $\Delta = \Delta_{\text{pre}} + \Delta_{\text{tr}} + \Delta_{\text{post}}$.

Therefore, the optimal solution so as to minimize the UEC can be given by

$$\Psi = \mathbf{W}^{-1}\mathbf{H}. \tag{30}$$

As a result, the analytic solution of the energy-efficient CoM trajectory is obtained. Obviously, it can be used for 3MIPM when considering (16).

3.3. Constrained ZMP movement optimization

Following the idea in ref. [42], the ZMP reference can be optimized to further reduce the UEC, where the feasibility constraints are taken into consideration. This section will briefly introduce the cost function, feasibility constraints, and search policy.

https://doi.org/10.1017/S0263574720001320 Published online by Cambridge University Press

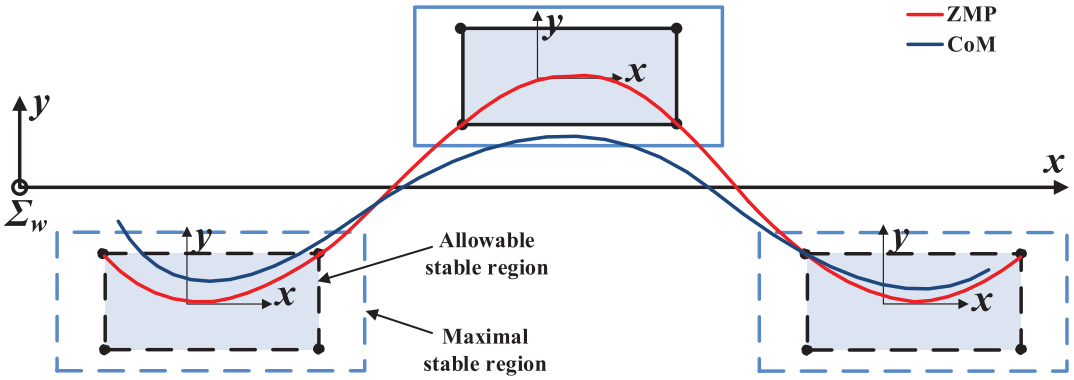

Fig. 5. ZMP support region formed by supporting foot.

3.3.1. Objective function. To evaluate the energetic cost accurately, the mechanical work needed by multiple joints is chosen as the cost function, which is calculated as

$$E_{\mathrm{m}} = \int_{T_1}^{T_2} \sum_{j=1}^{N_{\mathrm{f}}} \tau_j \dot{q}_j dt, \tag{31}$$

where τ_j and $\dot{q}_j$ represent joint torque and angular velocity, respectively, N_{f} represents the total number of joints, and T_1 and T_2 represent the beginning time and ending time of the whole walking process, respectively.

Note that angular velocity can be calculated by inverse kinematics (IK), while joint torque can be calculated by inverse dynamics (ID), as illustrated in Fig. 4.

3.3.2. Feasibility constraints. To generate the feasible gaits, physical constraints should be taken into consideration.

(1) *Constraints of ZMP movement* The robot can walk stably by restricting the ZMP within the maximal stable region, which is simplified as a polygon, as illustrated in Fig. 5. At present, we merely consider the ZMP motion during SSP. Thus, we can define linear inequality constraints for restricting ZMP motion. More details can be found in ref. [42]
(2) *Friction cone limitation* To avoid slippage when walking on the surface, the friction cone limitation is imposed, demanding that the tangential component of ground reactive force is sufficiently smaller than its normal element.
(3) *Constraints of mechanical structure and actuation capability* Due to the limitation of physical structure and actuation capability, the step parameters should be constrained. In this paper, we impose the linear inequality constraints on step length (L), step width (W), and step duration (T). In addition, the linear inequality constrains are also imposed on the variation of joint angle and angular velocity.

3.3.3. Search strategy. Since the 2nd-order polynomial is used to characterize the ZMP motion, two boundary conditions should be defined. To do this, we define the AZR as polygons, as illustrated in Fig. 5. Furthermore, we assume that the AZR polygon takes a certain percentage (we call it AZR percentage) of the maximal stable region. As a result, we define the following conditions to determine the ZMP trajectory during one natural walking cycle, which are expressed as

$$\begin{gathered} p_x(0) = \eta p_x^{\min}, \quad p_x(T_{\mathrm{s}}) = \eta p_x^{\max}, \quad \dot{p}_x(0) = (p_x(T_{\mathrm{s}}) - p_x(0))/T_{\mathrm{s}}, \\ \begin{cases} p_y(0) = p_y(T_{\mathrm{s}}) = \eta p_y^{\min}, & \textit{right support}, \\ p_y(0) = p_y(T_{\mathrm{s}}) = \eta p_y^{\max}, & \textit{left support}, \end{cases} \quad \dot{p}_y(0) = -\beta p_y(0)/T_{\mathrm{s}}, \end{gathered} \tag{32}$$

where η is the AZR percentage, β is the velocity coefficient that controls the ZMP trajectory along the $y-$axis.

https://doi.org/10.1017/S0263574720001320 Published online by Cambridge University Press

Algorithm 1: Constrained ZMP movement optimization

Input: step parameters: T, L, W
for ($\eta = 0.2$; $\eta = \eta + 0.1$; $\eta <= 0.8$) **do**
  Calculate mechanical work boundaries using (31):
    $E^{\min} \rightarrow E(\beta_{\text{ini}}^{\min})$, $E^{\max} \rightarrow E(\beta_{\text{ini}}^{\max})$;
  Iteration number $N_x \rightarrow 1$;
  while ($|\beta^{\max} - \beta^{\min}| \geq \varepsilon_{\beta}$ *and* $|E^{\max} - E^{\min}| \geq \varepsilon_{E}$ *and* $N^{\max} \geq N_x$) **do**
    update β: $\beta_{N_x} \rightarrow (\beta^{\min} + \beta^{\max})/2$;
    calculate mechanical work $E(\beta_{N_x})$ using (31);
    if *constrains in Section 3.3.2 are satisfied* **then**
      $\beta^{\max} \rightarrow \beta_{N_x}$;
      $E^{\max} \rightarrow E(\beta_{N_x})$;
    else
      $\beta^{\min} \rightarrow \beta_{N_x}$;
      $E^{\min} \rightarrow E(\beta_{N_x})$;
    end
    $N_x \rightarrow N_x + 1$;
  end
  Output: optimum $E_{\text{opt}} = E^{\min}$, $\beta_{\text{opt}} = \beta^{\min}$
end

As can be seen from (32), the reference ZMP trajectory is fully determined by η and β. Using (32), not only the AZR is optimized but also lateral CoM sway can be suppressed. Thus, under each parameter configuration (consisting of step duration (T), step length (L), and step width (W)), AZR percentage (η) and velocity coefficient (β) are optimized to achieve higher energy economy. Analysis in ref. [42] reveals that a smaller β (in the algebraic meaning) contributes to a smaller UEC. Therefore, to find the optimal β, we first set a constant η and then search the optimal β using the dichotomy method. The overall procedure is shown in Algorithm 1.

In Algorithm 1, N_x is the number of current iteration and $N^{\max}$ is the maximal iteration number. $\beta^{\max}$ and $\beta^{\min}$ are the upper and lower boundaries of velocity coefficient. The initial ones ($\beta_{\text{ini}}^{\max}$ and $\beta_{\text{ini}}^{\min}$) are tuned by hand so that the $\beta_{\text{ini}}^{\max}$ is feasible (if possible) and the $\beta_{\text{ini}}^{\min}$ is small enough to break the feasibility constraints. Therefore, the optimal feasible β can be searched. If there is not any feasible β under a specific η, the energetic cost of this loop is set to be a pre-defined value (E_r). Particularly, the $E(\beta_{N_x})$ denotes the mechanical work calculated by (31) with using β_{N_x}, E_{opt} and β_{opt} denote the optimal energetic cost and corresponding velocity coefficient under each group of step parameter configuration, respectively.

4. Simulation Results

This section evaluates the UEC performance of LIPM and 3MIPM by using the Nao-H25 robot platform, which contains 5 joints in each leg link. The basic algorithm parameters are listed in Table I (noting that at the ith cycle, we have $S_x = L$, $S_y = (-1)^{i+1} W$). For swing leg trajectory generation, the maximal clearance height was set to be 4 cm. In this section, the energy performance when using the unconstrained CoM optimization is first analyzed. Then, the two-stage AZR optimization is studied. Finally, after extending the approach in Section 3.2, the energetic benefit of BHV is demonstrated.

4.1. Bipedal walking when exploiting AZR

As mentioned in Section 1, three typical forms of ZMP trajectories, which are the fixed position during SSP without DSP (namely, instantaneous support switch), fixed position during SSP with DSP_{tr} and line trajectory during SSP with DSP_{tr}, have been studied by other researchers. In ref. [41], we proposed to make use of the parabolic ZMP reference so as to exploit AZR. In this work, we still assume rectangular AZR on each foot, which is 40 mm long and 30 mm wide. The time duration of DSP_{tr} (t_d) of each walking cycle, if exists, is 0.21 s. Note that we assume (c_{xb}, c_{yb}), (c_{xu}, c_{yu}), and (c_{xw}, c_{yw}) are zeros and (c_{zb}, c_{zu}, c_{zw}) equates to $Z_c/2$.

https://doi.org/10.1017/S0263574720001320 Published online by Cambridge University Press

Table I. Basic parameters.

Symbol	Description	Value
m_c	Total mass	5.12 kg
m_L	Leg mass	1.14 kg
m_B	Upper body mass	2.84 kg
l_b	Link length from hip to the center of body	50 mm
w_h	Hip width	85 mm
l_{th}	Link length from hip to knee	100 mm
l_{sh}	Link length from knee to ankle	103 mm
l_{ank}	Link length from ankle to foot plane	45 mm
Z_c	Fixed height of LIPM	310 mm
dt	Sampling time	0.01 s
T	Time duration of one UEWC	1.5 s
W	Absolute step width	100 mm
L	Absolute step length	60 mm

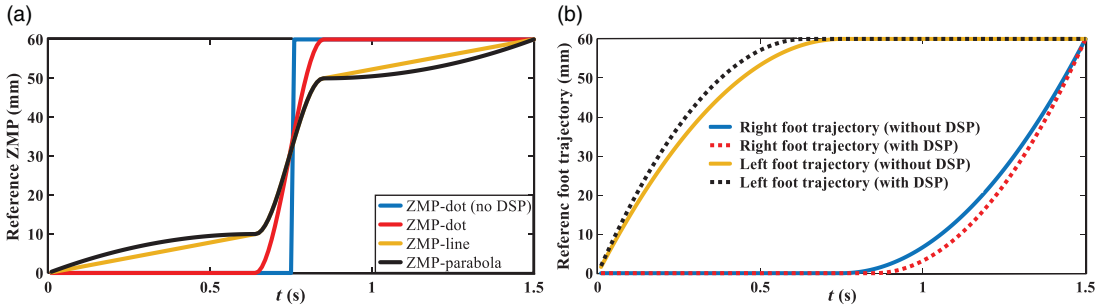

Fig. 6. Reference trajectories for 3MIPM, (a) ZMP references, (b) reference horizontal trajectories of swing foot center; 'ZMP-dot (no DSP)' represents the fixed ZMP position during the SSP with instantaneous support switch, 'ZMP-dot' represents the fixed ZMP position during the SSP with double support, 'ZMP-linear' represents the linear ZMP trajectory during the SSP with double support, 'ZMP-parabola' represents the parabolic ZMP trajectory during the SSP with double support.

4.1.1. Unconstrained trajectories generation. Tracking different ZMP references, the corresponding CoM trajectories are generated by using the method proposed in Section 3. Since ref. [41] has discussed the results generated by the LIPM in detail, this work focuses on the results of 3MIPM. Taking the forward motion as an example, the reference and generated trajectories within one UEWC are demonstrated in Figs. 6–8.

As illustrated in Fig. 6(a), four types of ZMP trajectories are chosen as references. Particularly, ZMP moves 10 mm during SSP_{pre} and SSP_{post} when using the linear and parabolic trajectories. As can be seen in Fig. 6(b), parabolic foot center trajectories are designed to synthesize the CoM trajectories of the support and swing legs.

Under the reference trajectories, the equivalent ZMP trajectories are calculated by Eqs. (16) and (17). Compared Fig. 7(a) with Fig. 6(a), it is easy to find that, due to the mass distribution, the equivalent ZMP trajectories suffer larger movement and severer fluctuation than the reference. For example, when using the dot ZMP reference during the SSP without/with the double support ('ZMP-dot (no DSP)'/'ZMP-dot' in Fig. 7(a)), the ZMP moves backwards during the SSP_{pre} and SSP_{post}. As a result, on the one hand, the corresponding CoM moves backwards at the beginning stage of the SSP_{pre} and the ending stage of the SSP_{post}, as can be seen from the blue and red lines in Fig. 7(b). One the other hand, the initial and end velocities of one *UEWC* are less than zeros, see Fig. 7(d). Since we expect the initial velocity of the robot to be zero or consistent with the direction of walking in the real application, we will plan the startup motion, that is, the CoM trajectory, for hardware experiments by using the polynomial interpolation scheme. By doing this, we can obtain the feasible gait for the whole walking process without weakening the energetic benefit.

https://doi.org/10.1017/S0263574720001320 Published online by Cambridge University Press

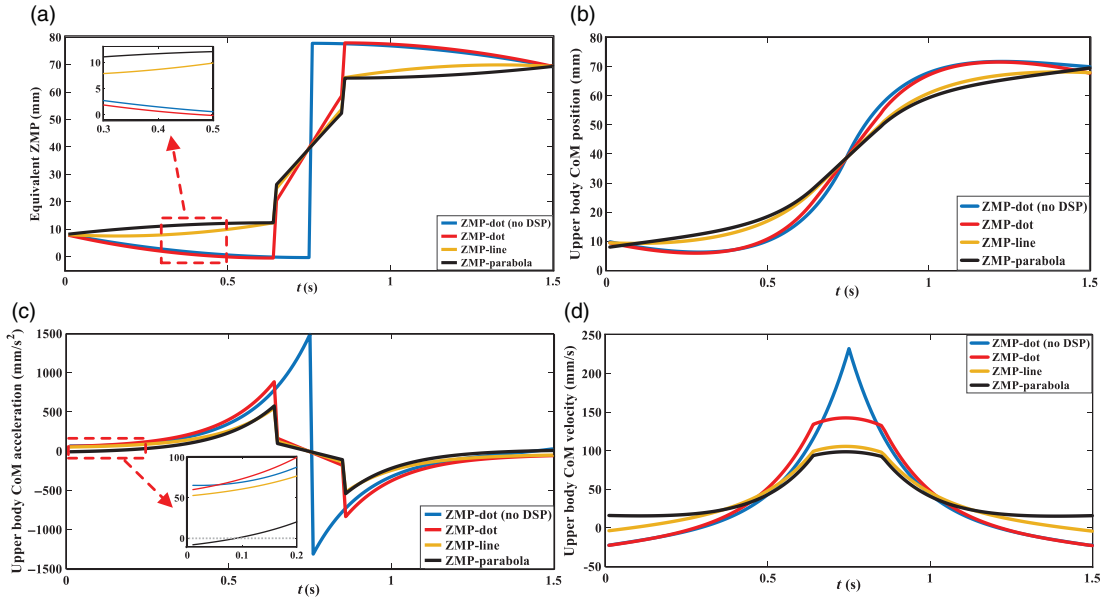

Fig. 7. Generate trajectories under different ZMP references.

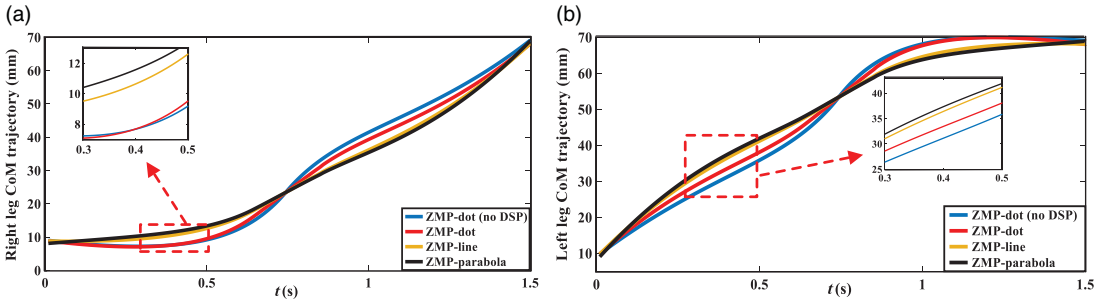

Fig. 8. Leg CoM Trajectories generation under different ZMP references, (a) right leg CoM trajectories, (b) left leg CoM trajectories.

Further observation on the CoM acceleration (the partial enlargement in Fig. 7(c)) and the CoM velocity (Fig. 7(d)) reveals that Eq. (2) is not strictly satisfied when using the first three forms of ZMP references, which is different from the result of LIPM. We believe it is because the leg mass is taken into consideration in the 3MIPM. Besides, when tracking the parabolic ZMP trajectory, Eq. (2) is not satisfied in particular time periods. However, these undesired periods merely last a very short duration. In other words, this case merely occurs at the beginning of SSP_{pre} and at the ending of SSP_{post}. Meanwhile, the CoM velocities and accelerations during these periods are quite low. Thus, the undesired case has a low impact on the overall energy performance.

In addition, as can be seen in Fig. 7(d), the upper body CoM velocities at the beginning and ending time are much less than those at the half time. That is, we can believe that Eq. (8) is satisfied. Therefore, the physical properties derived in Section 2.1.1 can also be applied upon the 3MIPM.

The leg mass trajectories synthesized by foot center trajectories and the upper body CoM trajectories are plotted in Fig. 8. As can be seen from Fig. 8, the right leg mass movement is merely determined by the upper body CoM trajectory during the SSP_{pre}, while the left leg mass movement is merely determined by the upper body CoM trajectory during the SSP_{post}.

Considering the mass distribution of 3MIPM, the generated CAOI and nominal energetic costs within one UEWC are calculated, which are listed in Table II. Note that the results of LIPM are also listed in Table II for the comparison. Numerical analysis reveals that, the least nominal energetic costs are obtained when tracking the parabolic ZMP reference, no matter the LIPM (E_{nom}) or 3MIPM (E^{3m}_{nom}) is used. Particularly, similar to the results of LIPM, when using the parabolic ZMP reference,

https://doi.org/10.1017/S0263574720001320 Published online by Cambridge University Press

Table II. Energetic costs needed by the forward motion.

Reference ZMP	J_C (10^4)	E_{nom} (10^4)	J_{C}^{3m} (10^4)	E_{nom}^{3m} (10^4)
Dot (no DSP)	16.02	14.57	33.47	17.52
Dot	6.24	6.23	13.48	7.44
Line	2.34	3.44	5.40	4.31
Parabola	2.10	2.96	4.67	4.00

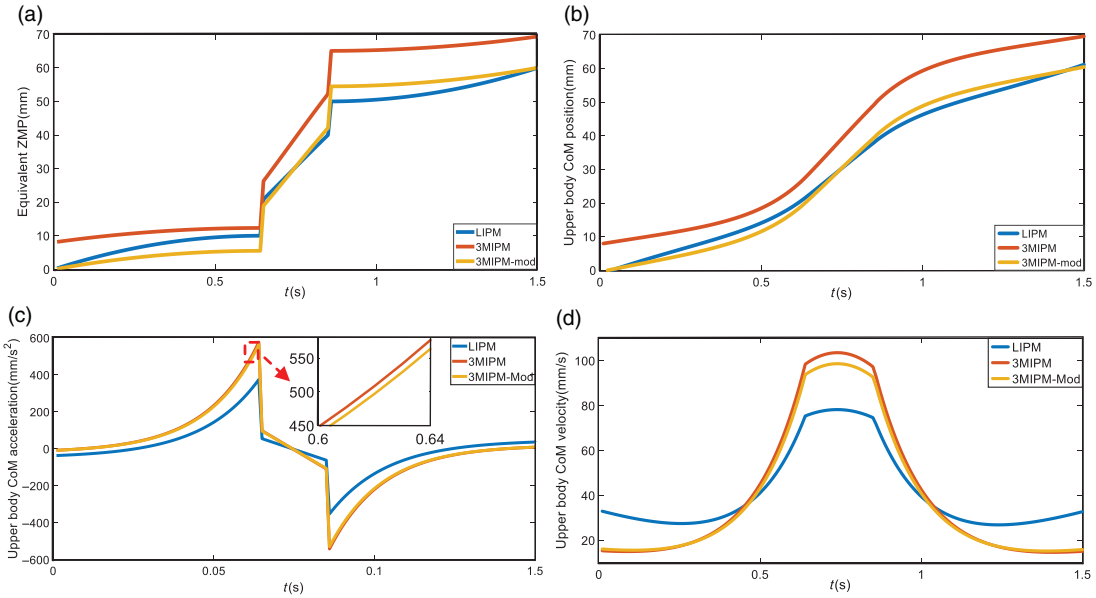

Fig. 9. Generated equivalent ZMP trajectories and CoM trajectories by different strategies.

the least CAOI of 3MIPM is also obtained. That is, the J_{C}^{3m} derived in Section 2.2.2 can be used to characterize the energetic cost of 3MIPM.

Due to the leg sway, the equivalent ZMP trajectories generated by the 3MIPM suffer more movements, leading to additional CoM movement (Fig. 7(b)) and extra energetic cost (Table II). As can be seen from Table II, when tracking the parabolic ZMP reference, the E_{nom}^{3m} (4.00) is much larger than E_{nom} (2.96). It should be noted that we should not compare the J_{C}^{3m} with the J_{C} for evaluating energy performances of different models since the mass distribution is considered in the 3MIPM but not in the LIPM.

4.1.2. Energy performance. The total nominal energetic costs of LIPM and 3MIPM are compared by taking into account the sagittal and coronal motions.

Defining the reference ZMP which is determined by the nominal step length, step width and expected ZMP movement during the SSP, the equivalent ZMP trajectory generated by the 3MIPM suffers more movement. Under the equivalent ZMP trajectory, the corresponding step length and step width (called the *equivalent step length* and *equivalent step width*) would differ from the nominal ones, which can be inferred from the red line in Fig. 9(a). As a result, more energetic cost is needed. In this work, to reduce the energetic cost, a search algorithm (we call it the *3MIPM-mod*) was proposed. Using this algorithm, the step length and width inputs are modified until the generated *equivalent step length and width* are close enough to nominal ones. Consequently, to generate 60 mm equivalent step length, the step length is adjusted to be 58 mm. The equivalent ZMP trajectories and (upper body) CoM trajectories generated by different strategies are illustrated in Fig. 9(a) and (b), respectively. Furthermore, the CoM velocity and acceleration are also adjusted, see Fig. 9(c) and (d). It should be mentioned that, compared with the single-mass model, the CoM keeps accelerating during the first

https://doi.org/10.1017/S0263574720001320 Published online by Cambridge University Press

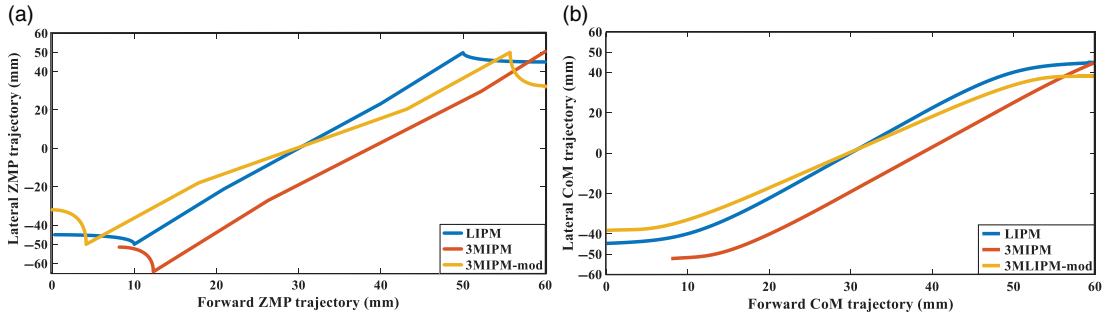

Fig. 10. Generated equivalent ZMP trajectories and optimal CoM trajectories, (a) equivalent ZMP trajectories (the parabolic ZMP reference of the LIPM is plotted as a comparison), (b) generated CoM trajectories.

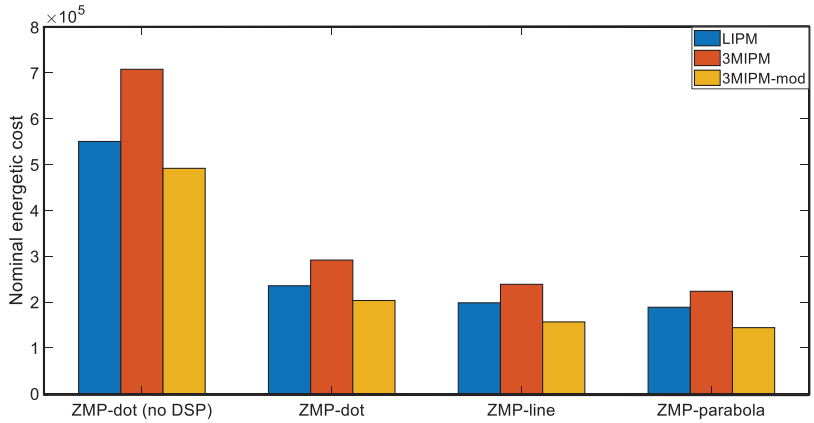

Fig. 11. Nominal energetic costs generated by different models under different ZMP references.

half UEWC and keeps decelerating during the late half UEWC when using the three-mass model (see Fig. 9(d)), meaning that the *CAOI* is more accurate when using the three-mass model. Besides, the maximal upper body acceleration and maximal velocity are both reduced when using 3MIPM-mod, meaning less energetic cost.

To further demonstrate the energetic benefit, the lateral motion is also taken into consideration. In this case, the step width input is adjusted to be 78 mm so as to generate equivalent 100 mm step width. The generated trajectories are illustrated in Fig. 10. In addition, the nominal energetic cost are calculated and plotted in Fig. 11. Again, under the parabolic ZMP trajectory, the energetic cost is reduced dramatically, no matter which model is used. Specifically, when using the 3MIPM-mod approach, the energetic cost when tracking the parabolic ZMP reference was reduced to be 29.3% of that when tracking the dot ZMP reference without DSP. Furthermore, using the 3MIPM-mod strategy, the minimal energetic cost was obtained compared with the other two models, no matter which form of ZMP reference is used. Taking the result under the parabolic ZMP reference as an example, the energetic cost generated by the 3MIPM-mod decreased by 23.6% when compared with that generated by LIPM and decreased by 35.5% when compared with that generated by 3MIPM.

4.2. Energy performance evaluation by two-stage optimization

To make better use of AZR, the two-stage optimization strategy introduced in Section 3.3 is utilized whereby CoM trajectory and ZMP reference are both adjusted. Differing from ref. [42], in this work, we focus on the energy performance w.r.t AZR percentage (η) and velocity coefficient (β).

4.2.1. Energy performance analysis by exploiting AZR. Defining the step length 60 cm, step width 100 mm, step duration 0.8 s, the energetic cost tracking a desired walking distance (500 mm in this case) is determined by the AZR percentage (η) and velocity coefficient (β). In this section, the variation of DSP ratio (δ) is also considered, varying from 0.2 to 0.8. The optimal velocity coefficient (β_{opt}) and energetic cost E_{opt} are demonstrated in Fig. 12.

https://doi.org/10.1017/S0263574720001320 Published online by Cambridge University Press

Table III. Optimal mechanical work generated by the two-stage optimization when using different models.

AZR percentage	**LIPM**		**3MIPM-mod**	
η	E_{opt} **(J)**	β_{opt}	E_{opt} **(J)**	β_{opt}
0.2	116.23	−11.97	135.54	−8.81
0.3	110.33	−7.27	120.61	−5.17
0.4	105.98	−4.92	108.63	−3.35
0.5	102.22	−3.51	99.82	−2.25
0.6	99.31	−2.57	93.16	−1.53
0.7	97.09	−1.90	89.14	−1.01
0.8	96.01	−1.39	94.99	−0.14

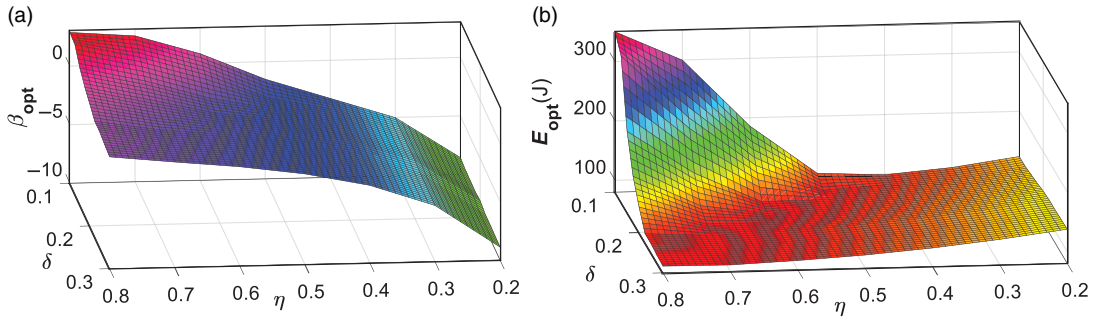

Fig. 12. Optimal velocity coefficient (a) and mechanical work (b) generated by two-stage optimization.

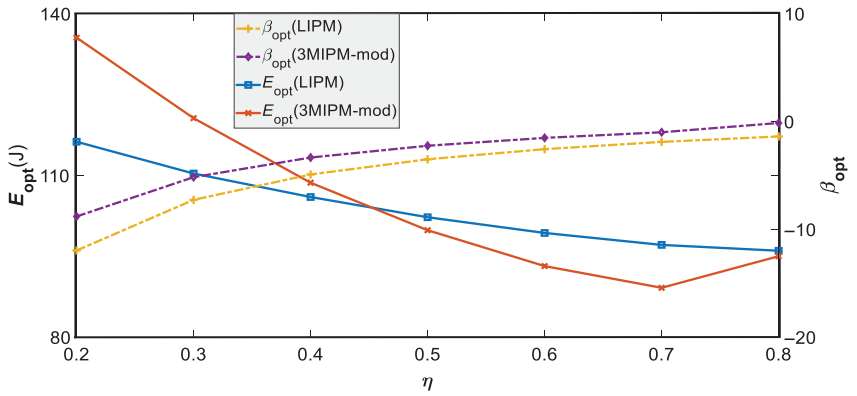

Fig. 13. Optimal mechanical work and velocity coefficient generated by the two-stage optimization when using different models.

As can be seen from Fig. 12(a), β_{opt} increases dramatically as η varies from 0.2 to 0.8. However, the E_{opt} does not behave in the same manner. Particularly, when $\delta > 0.2$, the E_{opt} keeps dropping as η rises, meaning that the utilization of AZR contributes to higher energy economy. Besides, using the same AZR percentage η, the β_{opt} decreases slightly as δ increases from 0.1 to 0.3. When $\eta < 0.6$, the E_{opt} almost keeps the same even the δ varies much. That is to say, using the 3MIPM-mod, the variation of minimal energetic cost is more sensitive to the change of AZR percentage, rather than the DSP ratio.

4.2.2. 3MIPM-mod versus LIPM. Assuming DSP ratio $\delta = 0.25$, the energy performances of different models are compared. As listed in Table III, the feasible β varies as the η changes so as to meet the physical constraints stated in Section 3.3.2. Particularly, β_{opt} increases gradually as the η rises, see the purple dash-dot line in Fig. 13. As a result, when η is smaller than 0.7, the total energetic cost (E_{opt}) reduces dramatically. When η is bigger than 0.7, the E_{opt} grows up due to the large velocity coefficient.

https://doi.org/10.1017/S0263574720001320 Published online by Cambridge University Press

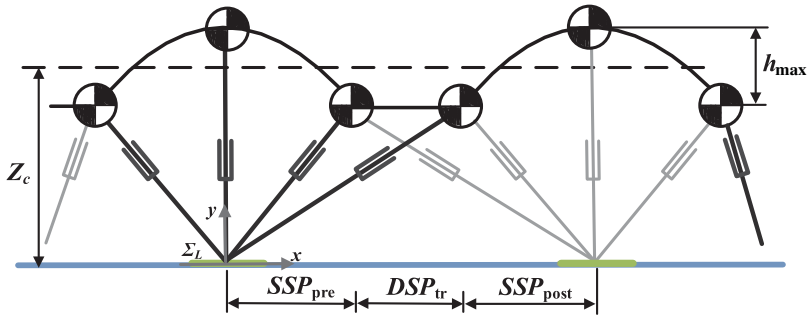

Fig. 14. IPM motion with body height variation: the vertical trajectory is determined by Z_c and h_{max}.

Compared with the LIPM, the 3MIPM-mod can achieve higher energy efficiency when $\eta > 0.4$. This is because that the velocity coefficient can be smaller enough (that is, close enough to the result of LIPM, see the purple dash-dot and yellow dash-dot lines in Fig. 13) in these circumstances. On the contrary, when $\eta < 0.4$, the β generated by the 3MIPM-mod would be much higher than the result of LIPM, leading to more energetic cost.

4.3. Bipedal walking when using BHV

Vertical height variation is another way contributing to lower energetic consumption.[36] In this section, the bipedal walking with BHV is discussed.

4.3.1. CoM trajectories generation. To simplify the problem, we assume parabolic CoM height reference that is asymmetric during the SSP_{pre} and SSP_{post}, as illustrated in Fig. 14. In addition, the velocity at the peak height is set to be zero. Thus, taking the height movement during SSP_{pre} as an example, we have

$$z(0) = Z_c + h_{max}/2, \quad z(t_i) = Z_c - h_{max}/2, \quad \dot{z}(0) = 0. \tag{33}$$

Since the vibration amplitude (h_{max}) is very low when compared with the stable component of height trajectory (Z_c), we merely modify the natural frequency when solving Eqs. (16) and (17). Considering the symmetry of CoM height during SSP_{pre} and SSP_{post}, the modified natural frequency (w_m^{eq}) during one UEWC becomes

$$w_m^{eq} = \sqrt{\frac{(g + C)(m_B + m_L)}{E_z m_c}}, \tag{34}$$

where C is the constant acceleration of height trajectory.

As a consequence, the method proposed in Section 3 can also be used to obtain the optimal CoM trajectory of 3MIPM when considering BHV. Besides, the 3MIPM-mod proposed in the last section can also be utilized to further improve the energy performance.

4.3.2. Energy performance. Firstly, to demonstrate the effectiveness of the proposed CAOI, the energy performance under the parabolic ZMP reference is analysed, by using four height trajectories. The upper-body CoM positions and accelerations generated by using different height trajectories are illustrated in Fig. 15, while the energetic costs are listed in Table IV. As can be seen from Table IV, the nominal energetic cost is reduced as the average height (Z_c) and vibration amplitude (h_{max}) increases, no matter which model is used. That is to say, the BHV contributes to higher energy economy. Besides, the CAOI expressed in Eqs. (9) and (14) is both reduced when considering height variation. Thus, the proposed CAOI is again demonstrated to be effective for UEC evaluation.

Then, focusing on the 3MIPM, the energy performance of bipedal walking with BHV when tracking different ZMP references is studied, and the total nominal energetic costs calculated by the 3MIPM-mod are demonstrated in Fig. 16. As can be seen from Fig. 16, the utilization of the ZMP movement during the SSP leads to less energetic cost, which is similar to the rules revealed in Section 4.1.2. Further analysis reveals that the energy performance depends much on the average

https://doi.org/10.1017/S0263574720001320 Published online by Cambridge University Press

Table IV. Energetic cost generated by using BHV under the parabolic ZMP reference.

Z_c+h_{max} (mm, mm)	J_C (10^4)	E_{nom} (10^4)	J_C^{3m} (10^4)	E_{nom}^{3m} (10^4)
310+0	39.31	35.05	52.08	28.82
310+20	38.84	34.79	51.45	28.62
320+0	37.79	34.24	50.18	28.21
320+20	37.34	33.99	49.56	28.02

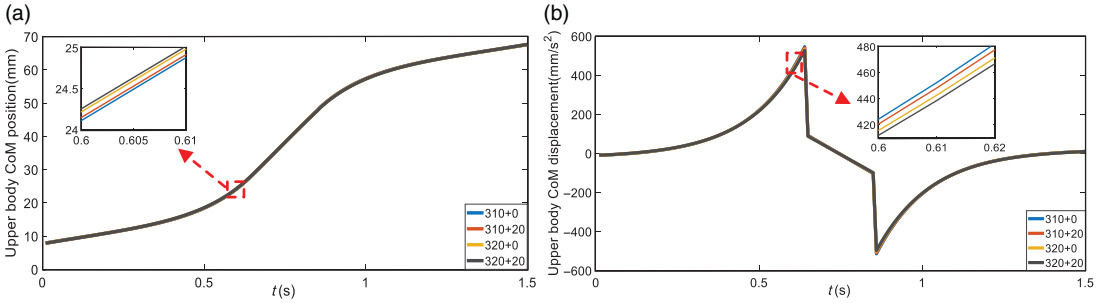

Fig. 15. Upper body CoM positions and accelerations generated by using different vertical height trajectories.

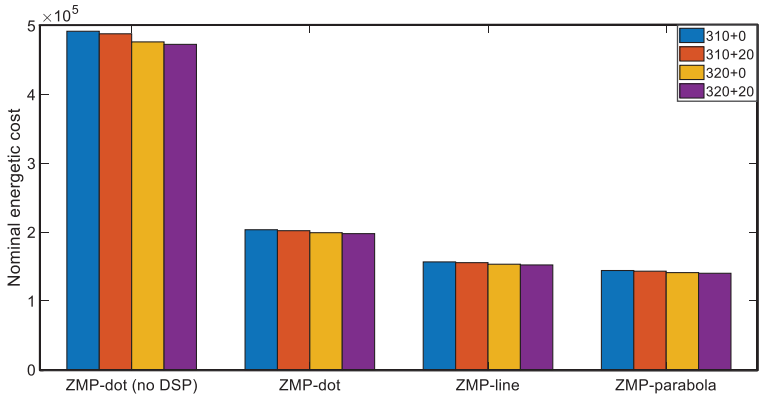

Fig. 16. Nominal energetic cost of 3MIPM-mod when using BHV under different ZMP references.

height (Z_c), which implies that the energetic cost would be reduced dramatically when walking with the straight knee.

5. Hardware Experiments

In the above sections, we focus on UEC evaluation by ignoring the energy loss caused by the friction work, gear transmission and other factors, bringing in modeling errors in energetic cost evaluation. Through hardware experiments, the total energetic consumption can be fully estimated by calculating the electrical energy cost. The total electrical energetic consumption (E_T) during the whole walking process is calculated by

$$E_T = \sum_{j=1}^{N_f} \int_{T_1}^{T_2} U_j I_j dt, \tag{35}$$

where U_j and I_j represent actual electric voltage and electric current on each motor, respectively, N_f is the total number of joints on both legs, T_1 and T_2 are the beginning time and ending time of the walking process, respectively.

https://doi.org/10.1017/S0263574720001320 Published online by Cambridge University Press

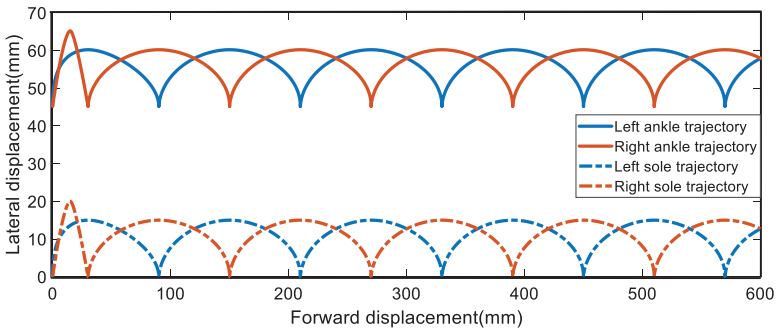

Fig. 17. Reference leg center trajectory for bipedal walking.

5.1. Experimental environment setup

Considering the undesired acceleration property at the beginning and the ending of one UEWC, as mentioned in Section 4.1.1, the startup motion and braking motion of the whole walking process are designed by a polynomial interpolation scheme for the stable walking. As a result, the average electric work when walking from 50 to 550 mm is computed so as to compare the energy performance of different models. Furthermore, to reduce the statistical error, the walking test under each group of parameters is repeatedly for 5 times and the average result is used as the actual energetic cost. In each case, the total energetic costs when using LIPM and 3MIPM-mod are calculated and compared. Note that, the preview control strategy proposed in ref. [51] is utilized for ZMP tracking. Furthermore, to reduce the trunk rotation, a PD controller is adopted to keep the body upright.

On a 3.0 GHz quad-core CPU, the time cost of each loop, including two-stage optimization and IK solution is less than 5 ms. Thus, the proposed method can be used in real time.

5.2. Experimental results

5.2.1. Bipedal walking when using AZR. In this section, only the ZMP references with double support are utilized. In this case, we set the average height 310 mm, step length 60 mm, step width 100 mm, step cycle 1.5 s, DSP ratio 0.15. It turned out that the robot could walk stably by tracking the reference leg trajectory (see Fig. 17) and ZMP trajectory (see Fig. 18). To obtain the energy-efficient gait and reduce the landing impact as well, the leg trajectory is generated by the 8th polynomial where the desired position, zeros velocity, zero acceleration at the initial, middle, and ending time of one cycle are chosen as boundary conditions. In addition, in Fig. 18, the actual ZMP trajectory, CoM trajectory, and foot locations of the 3MLIPM-mod when using parabolic ZMP trajectories are also demonstrated. As can be seen from Fig. 18, due to the integration of the preview control, the actual ZMP trajectory can track the reference so that the walking stability is guaranteed. Furthermore, the fluctuation of CoM trajectory is also suppressed to guarantee an accurate assessment of energy efficiency.

In terms of energetic consumption, we first study the actual electrical current. Taking the walking motion under the parabolic ZMP reference as an example, the actual electrical current of the knee joints is demonstrated in Fig. 19. As can be seen from Fig. 19, the overall electrical current needed by the right and left knee joint are reduced when using the 3MIPM-mod approach. Numerical analysis reveals that the mean value of the right knee current is 0.37A when using the 3MIPM-mod, whereas the mean value is 0.39A when using the LIPM. As a result, the energetic cost is reduced, as can be seen from Table V. Similar to Section 4, the minimal energetic cost is obtained when tracking the parabolic reference ZMP. Numerical analysis reveals that the actual energetic cost when tracking the parabolic reference ZMP is reduced to be 83.8% of that when tracking the dot reference when using LIPM and was reduced to be 81.8% when using 3MIPM-mod. Therefore, the experiments demonstrate the energetic benefit of AZR. Furthermore, it should be noticed that the energetic costs of LIPM are larger than those of 3MIPM-mod when using the same ZMP trajectory. That is to say, the hardware experiments demonstrated the energy economy of the three-mass model.

5.2.2. Bipedal walking with using BHV. Tracking the parabolic ZMP trajectory, the Nao robot can also keep balance when walking with height variance, whose energetic costs are listed in Table VI.

https://doi.org/10.1017/S0263574720001320 Published online by Cambridge University Press

Table V. Actual energetic cost needed by different ZMP references.

Reference	**LIPM**		**3MIPM-mod**	
ZMP	E_T**(J)**	**Ratio(%)**	E_T**(J)**	**Ratio(%)**
ZMP-dot	113.8	100	107.9	94.8
ZMP-line	106.5	93.6	98.8	86.8
ZMP-parabola	95.4	83.8	93.1	81.8

Table VI. Actual energetic cost using different height trajectories.

$Z_c + h_{max}$	**LIPM**		**3MIPM-mod**	
(mm,mm)	E_T**(J)**	**Ratio(%)**	E_T**(J)**	**Ratio(%)**
310+0	95.4	100	93.1	97.6
310+20	93.4	97.9	90.4	94.8
320+0	91.2	95.6	88.7	93.0
320+20	85.0	89.1	83.1	87.1

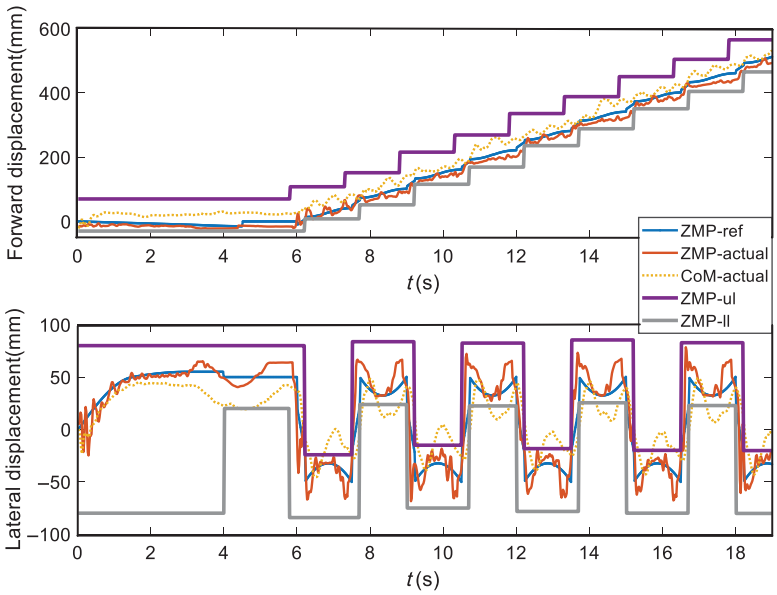

Fig. 18. Reference/actual ZMP and CoM trajectories of bipedal walking when using parabolic ZMP reference, 'ZMP-ul' and 'ZMP-ll' denote the upper boundary and lower boundary, respectively.

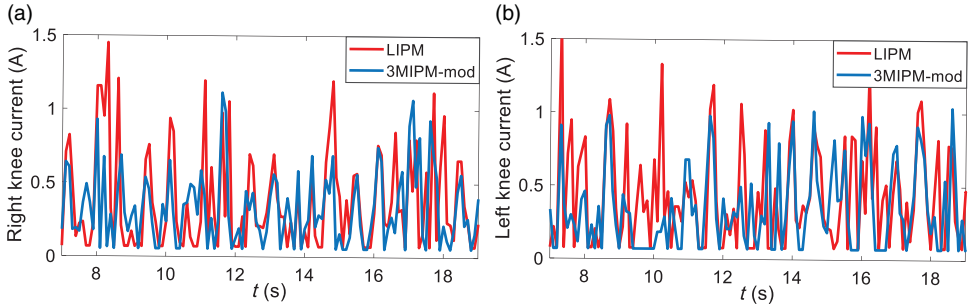

Fig. 19. Actual electrical current of the knee joints when using LIPM and 3MIPM models, (a) electrical current of the right knee joint, (b) electrical current of the left knee joint.

https://doi.org/10.1017/S0263574720001320 Published online by Cambridge University Press

As expected, the actual energetic consumption is also reduced as the average height and vibration amplitude increase. Further analysis reveals that using the LIPM, the actual energetic cost under the 320 mm + 20 mm height trajectory is reduced to be 89.1% of that under 310 mm + 0 mm height trajectory while is reduced to 87.1% when using the 3MIPM-mod approach. That is, when using the 3MIPM-mod, the higher energy economy is still achieved.

6. Conclusions

In this work, we derive a general CAOI for UEC evaluation, which can be utilized for the IPM and 3MIPM. Under the CAOI, by introducing the equivalent ZMP and equivalent natural frequency, a general unconstrained optimization approach is employed for obtaining the energy-efficient CoM trajectory, with the capability of tracking different forms of ZMP references and addressing the BHV. To make use of the AZR, a constrained optimization strategy is also adopted to adjust the ZMP reference.

Simulation and hardware experiments have demonstrated that the CAOI is valid for UEC evaluation. By employing the proposed strategy, we theoretically reveal the energetic benefit of the AZR through comparison studies on energy performance under different ZMP references. Results demonstrate that the parabolic reference ZMP trajectory is better than other commonly used ZMP references in energy saving, no matter IPM or 3MIPM is used. By employing the proposed CAOI, the energetic benefit of BHV is also demonstrated. Furthermore, in the above cases, by modifying the step parameters input, higher energy economy is also achieved by using the 3MIPM.

Extended works on leg movements optimization can be further employed in the future. Inspired by the idea of natural walking, learning from human demonstrations, especially the human-like knee joint movement would contribute to higher energy economy.

Acknowledgments

This work is supported by National Natural Science Foundation of China (Grant Nos. 51675385 and 51175383). Also, this paper is partially supported by funding 2019-ICP002 from the Shenzhen Institute of Artificial Intelligence and Robotics for Society.

References

1. J. Rose and J. Gamble, eds, *Human Walking*, 2nd ed. (Williams and Wilkins, Baltimore, MD, 1994).
2. Y. Sakagami, R. Watanabe, C. Aoyama, S. Matsunaga, N. Higaki and K. Fujimura, "The Intelligent Asimo: System Overview and integration," *Proceedings of the IEEE/RSJ International Conference on Intelligent Robots and Systems* (2002) pp. 2478–2483.
3. M. Fallon, S. Kuindersma, S. Karumanchi, M. Antone, T. Schneider, H. Dai, C. P. D'Arpino, R. Deits, M. DiCicco, D. Fourie and T. Koolen, "An architecture for online affordance-based perception and whole-body planning," *J. Field Robot* **32**(2), 229–254 (2015).
4. N. G. Tsagarakis, D. G. Caldwell, F. Negrello, W. Choi, L. Baccelliere, V. G. Loc, J. Noorden, L. Muratore, A. Margan, A. Cardellino and L. Natale, "Walk-man: A high-performance humanoid platform for realistic environments," *J. Field Robot* **34**(7), 1225–1259 (2017).
5. T. Kamioka, H. Kaneko, M. Kuroda, C. Tanaka, S. Shirokura, M. Takeda and T. Yoshiike, "Dynamic Gait Transition Between Walking, Running and Hopping for Push Recovery," *Proceedings of the IEEE-RAS International Conference on Humanoid Robotics* (2017) pp. 1–8.
6. J. Ding, Y. Wang, M. Yang and X. Xiao, "Walking stabilization control for humanoid robots on unknown slope based on walking sequences adjustment," *J. Intell. Robot Syst.* **90**(3–4), 323–338 (2018).
7. J. Ding, C. Zhou, Z. Guo, X. Xiao and N. Tsagarakis, "Versatile Reactive Bipedal Locomotion Planning Through Hierarchical Optimization," *Proceedings of IEEE International Conference on Robotics and Automation* (2019) pp. 256–262.
8. A. Shahrokhshahi, A. Yousefi-Koma, M. Khadiv, S. Mansouri and S. S. Mohtasebi, "Optimal stair climbing pattern generation for humanoids using virtual slope and distributed mass model," *J. Intell. Robot Syst.* **94**(1), 1–17 (2019).
9. A. D. Kuo, "Choosing your steps carefully," *Robot Autom. Mag.* **14**(2), 18–29 (2007).
10. S. Collins, A. Ruina, R. Tedrake, M. Wisse and M. Wisse, "Efficient bipedal robots based on passive-dynamic walkers," *Science* **307**(5712), 1082–1085 (2005).
11. W. L. Ma, A. Hereid, C. M. Hubicki and A. D. Ames, "Efficient HZD Gait Generation for Three-Dimensional Underactuated Humanoid Running," *Proceedings of IEEE/RSJ International Conference on Intelligent Robots and Systems* (2016) pp. 5819–5825.
12. Y. Cao, S. Suzuki and Y. Hoshino, "Uphill and level walking of a three-dimensional biped quasi-passive walking robot by torso control," *Robotica* **34**(3), 483–496 (2016).

13. W. Roozing, Z. Li, D. G. Caldwell and N. G. Tsagarakis, "Design optimisation and control of compliant actuation arrangements in articulated robots for improved energy efficiency," *IEEE Robot. Autom. Lett.* **1**(2), 1110–1117 (2016).
14. H. Q. Vu, X. Yu, F. Iida and R. Pfeifer,"Improving energy efficiency of hopping locomotion by using a variable stiffness actuator," *IEEE ASME Trans. Mechatron.* **21**(1), 472–486 (2016).
15. K. Sohn and P. Oh, "Applying Human Motion Capture to Design Energy-Efficient Trajectories for Miniature Humanoids," *Proceedings of IEEE/RSJ International Conference on Intelligent Robots and Systems* (2012) pp. 3425–3431.
16. T. Tomoyuki, Y. Azuma and T. Shibata, "Acquisition of Energy-Efficient Bipedal Walking Using CPG-Based Reinforcement Learning," *IEEE/RSJ International Conference on Intelligent Robots and Systems* (2009) pp. 827–832.
17. P. Kormushev, B. Ugurlu, D. G. Caldwell and N. G. Tsagarakis, "Learning to exploit passive compliance for energy-efficient gait generation on a compliant humanoid," *Auton. Robot.* **43**(1), 79–95 (2019).
18. V. H. Dau, C. M. Chew and A. N. Poo, "Achieving energy-efficient bipedal walking trajectory through GA-based optimization of key parameters," *Int. J. H. R.* **6**(4), 609–629 (2009)
19. S. J. Hasaneini, J. E. Bertram and C. J. Macnab, "Energy-optimal relative timing of stance-leg push-off and swing-leg retraction in walking," *Robotica* **35**(3), 654–686 (2017).
20. R. Zhang, H. Liu, F. Meng, R. Kang, Z. Yu, A. Ming and Q. Huang, "Energy Efficiency and Speed Optimization by Squad-Unit Genetic Algorithm for Bipedal Walking," *IEEE International Conference on Robotics and Biomimetics* (2018) pp. 661–667.
21. Y. Liang, Z. Liu and Y. Chen, "Energy efficient walking control for biped robots using interval type-2 fuzzy logic systems and optimized iteration algorithm," *ISA Trans.* **87**, 143–153 (2019).
22. K. An, Y. Liu, Y. Li, Y. Zhang and C. Liu, "Energetic walking gaits studied by a simple actuated inverted pendulum model," *J. Mech. Sci. Technol.* **32**(5), 2273–2281 (2018).
23. Z. Wang, G. Yan, Z. Lin, C. Tang and S. Song, "A switching control strategy for energy efficient walking on uneven surfaces," *Int. J. H. R.* **12**(04), 1550015 (2015).
24. C. Choi and E. Frazzoli, "Torque Efficient Motion Through Singularity," *Proceedings of IEEE International Conference on Robotics and Automation* (2017) pp. 5012–5018.
25. S. Hasaneini, C. Macnab, J. Bertram and H. Leung, "Optimal Relative Timing of Stance Push-Off and Swing Leg Retraction," *Proceedings of IEEE/RSJ International Conference on Intelligent Robots and Systems* (2013) pp. 3616–3623.
26. S. Kajita, O. Matsumoto and M. Saigo, "Real-Time 3D Walking Pattern Generation for a Biped Robot with Telescopic Legs," *Proceedings of IEEE International Conference on Robotics and Automation* (2001) pp. 2299–2306.
27. M. Brandao, K. Hashimoto, J. Santos-Victor and A. Takanishi, "Footstep planning for slippery and slanted terrain using human-inspired models," *IEEE Trans. Robot.* **32**(4), 868–879 (2016).
28. C. Santacruz and Y. Nakamura, "Walking Motion Generation of Humanoid Robots: Connection of Orbital Energy Trajectories via Minimal Energy Control," *Proceedings of IEEE-RAS International Conference on Humanoid Robots* (2011) pp. 695–700.
29. L. Lanari, S. Hutchinson and L. Marchionni, "Boundedness Issues in Planning of Locomotion Trajectories for Biped Robots," *Proceedings of IEEE-RAS International Conference on Humanoid Robots* (2014) pp. 951–958.
30. L. Lanari and S. Hutchinson, "Optimal Double Support Zero Moment Point Trajectories for Bipedal Locomotion," *Proceedings of IEEE/RSJ International Conference on Intelligent Robots and Systems* (2016) pp. 5162–5168.
31. M. Vukobratović and J. Stepanenko, "On the stability of anthropomorphic systems," *Math. Biosci.* **15**(1–2), 1–37 (1972).
32. K. Erbatur and O. Kurt, "Natural ZMP trajectories for biped robot reference generation," *IEEE Trans. Ind. Electron.* **56**(3), 835–845 (2009).
33. T. H. S. Li, Y. T. Su, S. H. Liu, J. J. Hu and C. C. Chen, "Dynamic balance control for biped robot walking using sensor fusion, kalman filter, and fuzzy logic," *IEEE Trans. Ind. Electron.* **59**(11), 4394–4408 (2012).
34. H. Zhu, M. Luo, T. Mei, J. Zhao, T. Li and F. Guo, "Energy-efficient bio-inspired gait planning and control for biped robot based on human locomotion analysis," *J. Bionic. Eng.* **13**(2), 271–282 (2016).
35. H. K. Shin and B. K. Kim, "Energy-efficient gait planning and control for biped robots utilizing the allowable ZMP region," *IEEE Trans. Robot.* **30**(4), 986–993 (2014).
36. Y. Ogura, K. Shimomura, H. Kondo, A. Morishima, T. Okubo, S. Momoki, H. O. Lim and A. Takanishi, "Human-Like Walking with Knee Stretched, Heel-Contact and Toe-Off Motion by a Humanoid Robot," *Proceedings of IEEE/RSJ International Conference on Intelligent Robots and Systems* (2006) pp. 3976–3981.
37. S. Omran, S. Sakka and Y. Aoustin, "Effects of com vertical oscillation on joint torques during 3D walking of humanoid robots," *Int. J. H. R.* **13**(4), 1650019 (2016).
38. R. J. Griffin, S. Bertrand, G. Wiedebach, A. Leonessa and J. Pratt, "Capture Point Trajectories for Reduced Knee Bend Using Step Time Optimization," *Proceedings of IEEE-RAS International Conference on Humanoid Robotics* (2017) pp. 25–30.
39. H. Zhu, M. Luo and J. Li, "Optimization-based gait planning and control for biped robots utilizing the optimal allowable ZMP variation region," *Ind. Robot* **45**(4), 469–489 (2018).

40. S. Kajita, M. Benallegue, R. Cisneros, T. Sakaguchi, S. I. Nakaoka, M. Morisawa, K. Kaneko and F. Kanehiro,"Biped Walking Pattern Generation Based on Spatially Quantized Dynamics," *Proceedings of IEEE-RAS International Conference on Humanoid Robotics* (2017) pp. 599–605.
41. J. Ding, C. Zhou and X. Xiao, "Energy-Efficient Bipedal Gait Pattern Generation via Com Acceleration Optimization," *Proceedings of IEEE-RAS International Conference on Humanoid Robots* (2018) pp. 238–244.
42. J. Ding and X. Xiao, "Two-stage optimization for energy-efficient bipedal walking," *J. Mech. Sci. Technol.* **34**(9), 3833–3844 (2020).
43. T. Sato, S. Sakaino and K. Ohnishi, "Real-time walking trajectory generation method with three-mass models at constant body height for three-dimensional biped robots," *IEEE Trans. Ind. Electron.* **58**(2), 376–383 (2011).
44. A. Albert and W. Gerth, "Analytic path planning algorithms for bipedal robots without a trunk," *J. Intell. Robot Syst.* **36**(2), 109–127 (2003).
45. T. Sato, S. Sakaino and K. Ohnishi, "Real-Time Walking Trajectory Generation Method at Constant Body Height in Single Support Phase for Three-Dimensional Biped Robot," *Proceedings of IEEE International Conference on Industrial Technology* (2009) pp. 1–6.
46. S. Shimmyo, T. Sato and K. Ohnishi, "Biped walking pattern generation by using preview control based on three-mass model," *IEEE Trans. Ind. Electron.* **60**(11), 5137–5147 (2013).
47. R. C. Luo and C. C. Chen, "Biped walking trajectory generator based on three-mass with angular momentum model using model predictive control," *IEEE Trans. Ind. Electron.* **63**(1), 268–276 (2016).
48. I. S. Kim, Y. J. Han and Y. D. Hong, "Stability control for dynamic walking of bipedal robot with real-time capture point trajectory optimization," *J. Intell. Robot Syst.* **96**(3), 1–17 (2019).
49. H. K. Shin and B. K. Kim, "Energy-efficient gait planning and control for biped robots utilizing vertical body motion and allowable ZMP region," *IEEE Trans. Ind. Electron.* **62**(4), 2277–2286 (2015).
50. J. Englsberger, C. Ott and A. Albu-Schäffer, "Three-dimensional bipedal walking control based on divergent component of motion," *IEEE Trans. Robot.* **31**(2), 355–368 (2015).
51. S. Kajita, F. Kanehiro, K. Kaneko, K. Fujiwara, K. Harada, K. Yokoi and H. Hirukawa,"Biped Walking Pattern Generation by Using Preview Control of Zero-Moment Point," *Proceedings of IEEE International Conference on Robotics and Automation* (2003) pp. 1620–1626.

https://doi.org/10.1017/S0263574720001320 Published online by Cambridge University Press